Ab initio elastic properties and tensile strength of crystalline hydroxyapatite

W.Y. Ching, Paul Rulis, Anil Misra

Ab initio elastic properties and tensile strength of crystalline hydroxyapatite

W.Y. Ching [a,*], Paul Rulis [a], A. Misra [b]

[a] Department of Physics, University of Missouri-Kansas City, Kansas City, MO 64110, USA
[b] Department of Civil, Environmental and Architectural Engineering, University of Kansas, Lawrence, KS 66045, USA

Received 14 March 2009; received in revised form 18 April 2009; accepted 23 April 2009

Abstract

We report elastic constant calculation and a "theoretical" tensile experiment on stoichiometric hydroxyapatite (HAP) crystal using an ab initio technique. These results compare favorably with a variety of measured data. Theoretical tensile experiments are performed on the orthorhombic cell of HAP for both uniaxial and biaxial loading. The results show considerable anisotropy in the stress–strain behavior. It is shown that the failure behavior of the perfect HAP crystal is brittle for tension along the z-axis with a maximum stress of 9.6 GPa at 10% strain. Biaxial failure envelopes from six "theoretical" loading tests show a highly anisotropic pattern. Structural analysis of the crystal under various stages of tensile strain reveals that the deformation behavior manifests itself mainly in the rotation of the PO_4 tetrahedron with concomitant movements of both the columnar and axial Ca ions. These results are discussed in the context of mechanical properties of bioceramic composites relevant to mineralized tissues.

Keywords: Hydroxyapatite; Mechanical properties; Elastic constants; Tensile strength

1. Introduction

Collagen and apatitic mineralites can form complex composite structures that have remarkable mechanical properties and are thus the two primary building blocks of most hard tissues [1,2]. Detailed and accurate structure–property–function relationships of apatitic mineralites, collagen and their composites are critically important for evaluating the mechanical properties of bone and dentin structures, for understanding diseased states of mineralized tissues, and for establishing biomimetic material-design principles. Most mineralized tissues, such as bone and dentin, are organized hierarchically in terms of composition, structure and properties, and they exhibit multiscale structure/property interdependence (molecule/crystallite to fibril to fiber, etc.). Over the decades, intense research has been performed to understand the behavior of these materials at different hierarchical scales [3–10]. The significant role that biological apatite(s) play in the structure and function of calcified tissues was recognized as far back as the early part of the last century [11]. The composition and crystal structure of biological apatite(s) and their implication for function have since been a subject of continuous investigation [11–15]. Recent investigations and data interpretations have also linked apatite composition properties to aging and disease [16,17].

Many computational and experimental studies performed at different spatial scales on a prototype bioceramic, hydroxyapatite (HAP), and the related carbonated HAP, which is more relevant to biological environments, have advanced our understanding of mineralized tissue. However, details of the atomic-scale interactions that are at the heart of the mechanical properties remain as critically missing pieces of information. Clearly, in the absence of such information our understanding of calcified tissue behavior will remain incomplete. Only recently have researchers begun to address the problem at this scale

* Corresponding author. Tel.: +1 816 235 2503.
E-mail address: chingw@umkc.edu (W.Y. Ching).

[18]. The various efforts to relate mineralized tissue mechanical properties to constituent phase show that simple consideration of composition is insufficient. One of us (A.M.) has recently performed homotopic (same location and lateral resolution) microscale density–composition–elastic modulus measurements on human dentin [19] and showed that, at the same mineral volume fraction and density, the elastic modulus can vary by as much as a factor of five. Similar results have also been found for bones and calcified cartilage based upon nanoindentation [20,21]. While qualitative and subjective explanations abound, there is a distinct absence of quantitative theories and reliable data.

The key obstacle hampering further progress is a lack of understanding of the mechanical behavior in terms of atomic-scale mechanisms. With recent advances in computational capabilities, it is now possible to investigate the mechanical behavior of complex multi-atom systems using large atomic models (of the order of 1000 atoms) and ab initio methods [22–25]. In this paper, we report the results of the mechanical properties of stoichiometric HAP crystal using a highly accurate ab initio technique. The goal is to demonstrate that the atomic structure has a large influence on the anisotropy of the mechanical behavior, leading to significantly different failure behaviors. Such data are crucial for explaining the directional dependence of the alignment of mineralites in collagen fibrils and is the first step towards deeper understanding of collagen/apatite composites that are important to the biological and biomedical community. The implication is that similar ab initio studies along these lines will provide important fundamental insights for furthering our understanding of the mechanical behavior of composite material at the tissue level.

In this work, we report the elastic constants and bulk properties of perfect crystalline HAP and have carried out uniaxial and biaxial "theoretical" tensile experiments to investigate the deformation and failure behavior of HAP under strain. We briefly outline the method of simulation in Section 2; Section 3 describes the results obtained and these results and their implications are further discussed in Section 4. The paper ends with some conclusions in Section 5.

2. Method of simulation

2.1. Crystal structure

The HAP crystal has a fairly complex structure with 44 atoms in the hexagonal primitive cell [26] (two formula units of $Ca_5(PO_4)_3OH$, space group $P6_3/m$ and a 50% partial occupancy of the OH sites). The crystal consists of tightly bonded PO_4 tetrahedral units, two types of Ca ions and the OH groups. The OH is aligned along the crystalline c-axis. There are two Ca sites, Ca1 and Ca2, that are usually labeled as columnar Ca and axial Ca, respectively, and which play the role of ionically bonding the PO_4 units together. For O ions, there are three crystallographically nonequivalent sites. O1 and O2 have 6 sites and O3 has 12 sites. In most bioceramics the Ca/P ratio is usually used to characterize the sample [27]. This value is 1.666 for stoichiometric HAP but the real samples in laboratory experiments usually can have Ca/P ratios either larger or smaller than this value, indicating the difficulty in obtaining pure samples for this quite common bioceramic material. In carbonated HAP, where the CO_3 group replaces the PO_4 group, the Ca/P ratio would be much higher due to the reduction of P. However, in most defective samples where vacancies or Ca deficiencies exist, the Ca/P ratio can be in the range of 1.5–1.67. In tri-calcium phosphate, $Ca_3(PO_4)_2$, another important bioceramic, the Ca/P ratio is 1.5.

The electronic structure and bonding of the HAP crystal has been studied by several groups in recent years [28–31]. We have also studied the surface structure and surface electronic structure of HAP and fluorapatite (FAP) crystals [30]. More recently, ab initio techniques have been used to explore the geometry of water molecules absorbed on the surfaces of the HAP crystal [32–34]. On the other hand, there has been very little computational effort devoted to the mechanical properties, presumably due to HAP's structural complexity and the accuracy required for computing ab initio mechanical properties at the atomistic level.

2.2. Elastic properties

HAP crystallizes in a hexagonal lattice (a, b and c axes) with the OH group oriented along the c-axis. For studying mechanical properties, it is more expedient to transform it into an orthorhombic cell (x, y and z axes) with the z-axis parallel to the c-axis as illustrated in Fig. 1. However, it is necessary to double the b-axis direction in order to maintain the periodicity of the lattice in the orthorhombic description. As a result, the simulation cell (hereafter

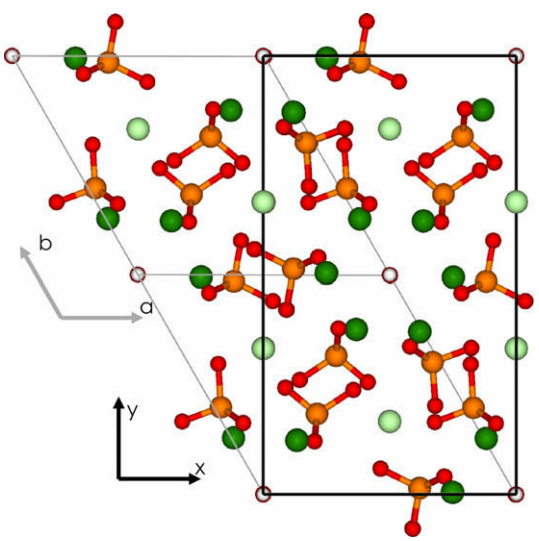

Fig. 1. Crystal structure of hexagonal and orthorhombic HAP. The light (heavy) green balls represent the columnar (axial) Ca ions. (For interpretation of the references to color in this figure legend, the reader is referred to the web version of this article.)

referred to as the supercell) is twice as large as the unit cell and contains 88 atoms. The [1 0 0] axis (x-axis) and the [0 1 0] axis (y-axis) are marked in Fig. 1 with the [0 0 1] axis (z-axis) orthogonal to the x–y axes.

To study the elastic properties of crystalline HAP, we first fully relax the orthorhombic supercell using the density functional theory based Vienna Ab initio Simulation Package (VASP) [35,36]. In the present calculation, we used the PAW-PBE potential [37] and a $2 \times 1 \times 3$ Monkhorst k-point sampling with an energy cut-off of 600 eV. The convergence criteria for the total energy and force per atom are set at 0.0001 eV and 0.001 eV Å^{-1}, respectively, to ensure high precision. Test calculations indicate that this level of accuracy is sufficient for accurate determination of the mechanical properties. The fully relaxed orthorhombic supercell has cell dimensions of $x = 9.5543$ Å, $y = 16.5507$ Å and $z = 6.8938$ Å. The volume of the cell is 1090.12 Å^3 which is only 1.23% smaller than twice the volume of the experimental hexagonal unit cell (1103.73 Å^3).

The elastic constants for the HAP crystal in the orthorhombic configuration are calculated based on the equilibrium structure and an in-house elastic tensor package specially designed for efficient evaluation of the stress–strain response [38]. Essentially, two strains ε_j of -1% and 1% are applied to each independent direction. The stress data (σ_i) are then collected from the fully relaxed structure under each strain. The nine elastic constants C11, C22, C33, C44, C55, C66, C12, C13 and C23 are extracted by solving the system of linear equations:

$$\sigma_i = \sum_{j=1}^{6} C_{ij}\varepsilon_j. \quad (1)$$

From the calculated elastic constants of the crystal, it is possible to extract the bulk structure parameters K (bulk modulus), G (shear modulus), E (Young's modulus) and η (Poisson's ratio). Although there are different approaches to obtain these bulk structural parameters, we have used the averaged values of the Voigt approximation [39] and the Reuss approximation [40]. The Voigt approximation assumes a uniform strain and gives the maximum bulk and shear modulus, whereas the Ruess approximation assumes a uniform stress and gives the minimum values of the same moduli. Hence, this so-called Voigt–Reuss–Hill (VRH) approximation [41] provides a more reliable estimation of bulk isotropic properties of the material based on the anisotropic elastic properties of a single crystal. The elastic constants and bulk structural parameters for a large number of ceramic crystals using this method have been reported in Ref. [38].

2.3. Tensile experiments

With vastly improved computational methodology and ever-increasing computing power, it is now feasible to perform "theoretical" tensile experiments to obtain reliable stress–strain data that are inaccessible to conventional laboratory experiments [42]. Such an approach has been successfully applied to investigate the failure behavior of complex ceramics containing microstructures such as internal grain boundaries [43] and intergranular glassy films [22,23]. In the present study for HAP, one of the axes of the orthorhombic supercell is extended stepwise in increments of 2%, while the lattice constants in the other two directions are fixed. This corresponds to the so-called uniaxial extension, rather than the uniaxial tension, and could introduce triaxial stress states [42]. During each extension step, the atomic positions in the supercell are fully relaxed using VASP. The extension steps are repeated for the next strain until the stress reaches the maximum and beyond. For the biaxial tensile experiment, two of the axes are simultaneously extended by an equal amount of strain with the lattice constant in the remaining direction kept fixed. It should be pointed out that the relaxation at each strain level to obtain the stable stress components of the cell is a fairly slow process for a large, complex supercell, especially after the maximum of the stress has been reached.

3. Results

3.1. Elastic constants and bulk structural parameters

The calculated elastic constants and bulk parameters using the VRH scheme are listed in Table 1 together with some available measured values. For an orthorhombic crystal, there are nine elastic constants: C11, C22, C33, C44, C55, C66, C12, C13 and C23. As expected, C11 is very close to C22 (140 and 135 GPa, respectively) in the orthorhombic cell description and C33 = 175 GPa is larger than C11. Snyders et al. [44] have also reported elastic constant calculations using VASP but used a different set of convergence criteria. Their C11 value is smaller than ours but the C33 value is much larger. The reported elastic constants from experimental measurements [44–52] on a variety of crystalline HAP samples via different techniques are listed in Table 1. The data for Ref. [46] is from bovine enamel but calculated using the model of Katz and Ukraincik [48]. On the whole, these data are closer to our calculated values than the calculated values of Ref. [44]. Our bulk structure parameters calculated from the elastic constants are: $K = 84.51$ GPa, $G = 47.77$ GPa, $E = 120.6$ GPa and a Poisson ratio of 0.262. These data are compared with the widely scattered measured data (see Table 1) on a variety of samples of different characters which may not correspond to perfectly stoichiometric HAP. In addition, the apparently large scattering of the measured data can be attributed to the different experimental techniques used to extract the elastic data. Our calculated values are in surprisingly good agreement with the work of Katz and coworkers [47,48], who measured the isotropic elastic constants of polycrystalline samples of HAP and FAP using ultrasonic interferometry coupled with a pressure-dependent apparatus to obtain the mechanical properties. These

Table 1
Elastic constants C_{ij} and bulk parameters (in GPa) of orthorhombic HAP. Experimental values are in parenthesis.

	Present work	Other calc.	Experiments		
		Ref. [44]	Ref. [45]	Ref. [46]	Refs. [47,48]
C11	140.0	117.1	166.7	115	137
C22	134.8				
C33	174.8	231.8	139.6	125	172
C44	47.5			22.8	
C55	47.6	56.4	66.3		
C66	48.2			36.6	
C12	42.4	26.2	13.1	42.2	42.5
C13	58.3	55.6	65.5	30.0	54.9
C23	60.1				
K	84.51	82		62	89
G	47.77			33	44.5
E	120.6	132.1			114
η	0.262	0.23	0.28 (c)	0.23 (d)	0.27

K from other experiments: 120 [49], 147 [44], 111 [50], 70–115 [51], 63–105 [52].

data are also much larger than those measured for cortical and trabecular bone by a factor of roughly 5–8 [53]. Our calculated values are for ideal crystal, and should therefore be considered as an upper limit.

3.2. Stress–strain relationship

The stress–strain results from the uniaxial tensile experiment are presented in Fig. 2 and those for biaxial extension are shown in Fig. 3. In each panel, there are three sets of data points corresponding to the calculated σ_{xx}, σ_{yy}, σ_{zz} components for loads in the *x*, *y*, *z* directions. It can be seen that the stress component in the loading direction is always the largest, but those in the other directions are also substantial. For loading in the *z*-direction, σ_{zz} is much larger than σ_{xx}, and σ_{yy}, which are identical since they are in the *x*–*y* plane of the HAP crystal. The maximum stress σ_{zz} in the *z*-direction is 9.6 GPa at the strain level of 10%. The strains for the maximum stresses in the *x*- and *y*-direction loading are approximately 14% and 16%, respectively. We note that there is a certain degree of uncertainly for these two values because the stress data near fracture (maximum stress) are relatively flat. As can be seen from Fig. 2, a gradual onset of failure akin to ductile behavior characterizes the stress–strain curves under *x*- and *y*-direction uniaxial extensions. Under *x*-direction uniaxial extension, the unit cell appears to "yield" at an axial stress of 6.7 GPa, corresponding to 8% strain, before reaching a peak axial stress of 7.4 GPa at 14% strain at which it exhibits softening. Similarly, under *y*-direction uniaxial extension, the unit cell appears to "fracture" at an axial stress of 8.6 GPa, corresponding to 10% strain, and reaches a peak axial stress of 9.1 GPa at 16% strain before exhibiting softening. In contrast, a brittle-like behavior characterizes the stress–strain curve under *z*-direction uniaxial extension.

The data for biaxial extension are shown in Fig. 3. All biaxial extensions show rather brittle failure patterns. The data in the *x*–*y* plane is quite different from those in the *y*–*z* and *z*–*x* planes. The strain at maximum stress is larger (12%) and the three components are almost the same at low strain. Data for the *y*–*z* and *z*–*x* planes are noticeably different and have the strain at a maximum stress of about 8%. Such behavior indicates strong anisotropy of the mechanical response in the HAP crystal.

3.3. Failure behavior

Since the HAP crystal shows "ductile" or "brittle" failure characteristics under different loading directions, it is difficult to devise a single failure criterion. From the viewpoint of a uniaxial failure criterion, we can consider the HAP crystal to have failed when the major principal stress reaches either a peak or a "yield" value under the various applied loading conditions. Based upon these criteria, the strain-to-failure along the *z*-direction is 10%, while those along the *x*- and *y*-axis are 8–14% and 10–16%, respectively. Thus, based upon the strain-at-the-peak-stress criterion, the *z*-direction would be considered to be the weakest. In comparison, based upon the "yield" stress criterion, the *x*-direction is the weakest. If we compare the principal stresses at failure, the HAP crystal fails at a lower stress under *x*-direction uniaxial extension irrespective of the failure criterion.

To further elucidate the failure behavior we have constructed biaxial failure envelopes in Fig. 4 by plotting the applied strain corresponding to the above failure criterion for the six "theoretical" loading tests performed in the present work. In the case of *x*- and *y*-direction uniaxial extensions, we have used both the peak stress as well as the "yield" stress criterion. The shaded area in Fig. 4 then represents the region of uncertain failure criterion.

From Fig. 4a we see that the failure behavior in the *x*–*y* plane is highly anisotropic both in terms of magnitude of strain-to-failure as well as the failure criterion. The failure envelopes in the *x*–*z* and *y*–*z* planes, shown in Fig. 4b and c, also exhibit directional dependency in terms of magni-

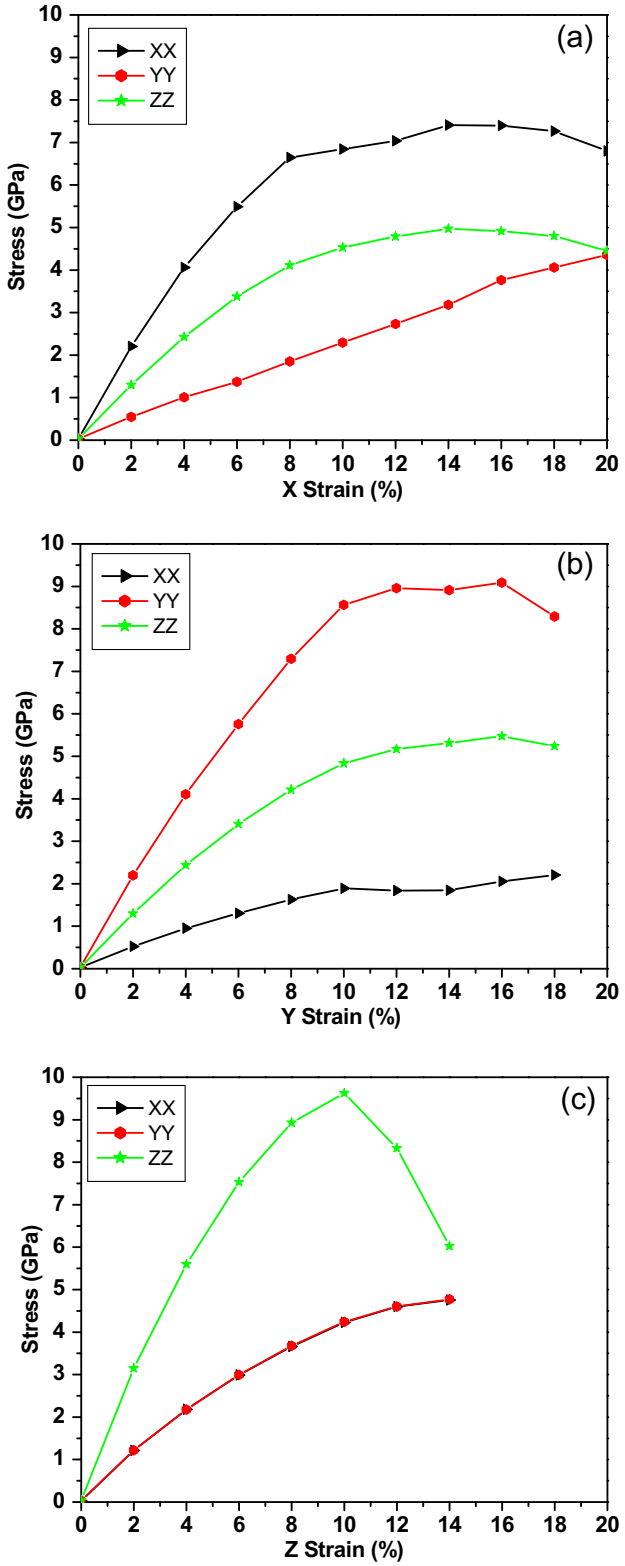

Fig. 2. Stress–strain data σ_{xx}, σ_{yy}, σ_{zz} for unixal loading in (a) the x-direction, (b) the y-direction and (c) the z-direction.

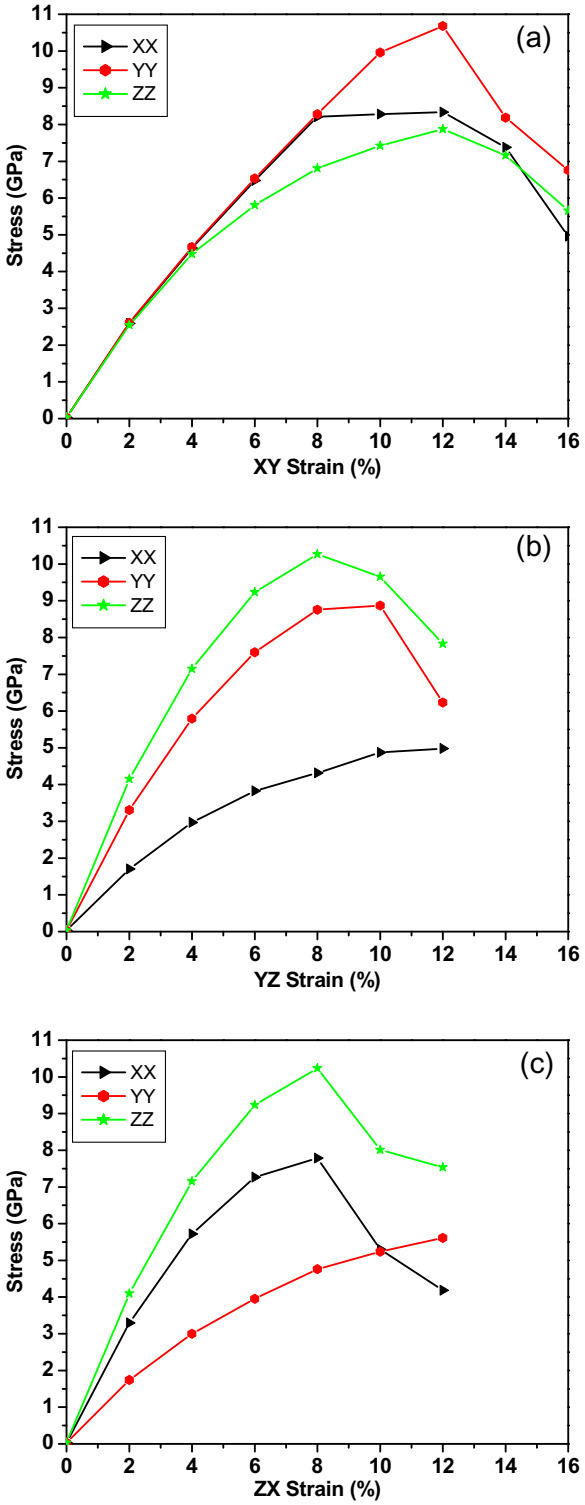

Fig. 3. Stress–strain data σ_{xx}, σ_{yy}, σ_{zz} for biaxial loading in (a) the xy-direction, (b) the yz-direction and (c) the zx-direction.

tude of strain-to-failure and the failure criterion. The failure envelopes indicate that the HAP crystal will show a brittle behavior under z-direction-dominated biaxial loading. The brittle behavior gradually transitions to a ductile behavior as the biaxial loading becomes dominated by the x-direction or y-direction.

As expected, these strain–space failure envelopes show a highly anisotropic behavior. Notably, the failure anisot-

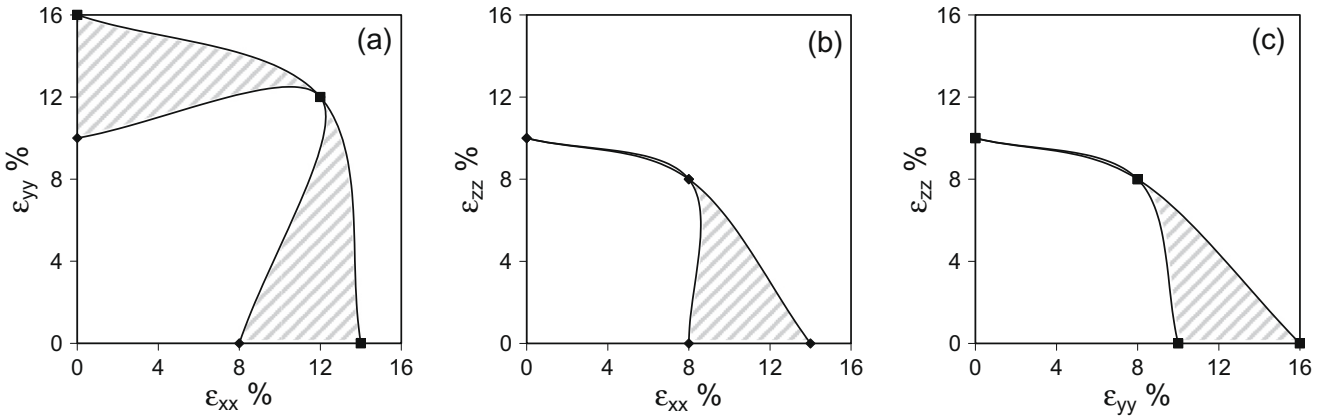

Fig. 4. Biaxial failure envelope plotted in the strain space for (a) the x–y plane, (b) the x–z and (c) y–z planes of the orthorhombic periodic cell. The shaded area represents the failure region since the x- and y-directions do not show a clear peak stress.

ropy in the x–y plane is in contrast to the calculated isotropic elastic behavior in the x–y plane. Since the x–y plane corresponds to the a–b crystallographic plane of the hexagonal cell, the elastic behavior is expected to be isotropic in that plane. In general, the anisotropy of the failure behavior does not coincide with the elastic anisotropy of HAP crystal. Such a behavior is probably due to the structural changes the crystal undergoes during loading.

To illustrate the structural changes under uniaxial strain, we show in Fig. 5 the atomistic structures of HAP in the y–z plane and the x–y plane at five different loading strains in the z-direction, including the structure for the equilibrium configuration of zero strain. At low strain, there is hardly any observable change in the atomistic structures. At high strain and after the maximum stress was reached, there are observable changes in the Ca ions (both columnar Ca and axial Ca) associated with the rotation of the tetrahedral PO_4 units. The lattice extension in the z-direction affects the interatomic interactions which cause the atoms to move into positions of minimum local stress, and this is most clearly manifested in the rotation of the tetrahedral PO_4 units. This could imply that one way to enhance the mechanical properties of HAP is to prevent the rotation of PO_4 tetrahedra. This can perhaps be achieved by strategic substitution of PO_4 by CO_3 group in the crystal or by other ways in forming interfacial structures. The carbonate group CO_3 has a pyramidal structure which has a lower rotational symmetry and requires more energy to rotate than the higher-symmetry tetrahedral PO4 group it replaces. This could conceivably be what is happening in the collagen/HAP composite materials. An interesting observation is that the alignment of the OH group along the c-axis is unchanged at strains for the z-direction extension.

4. Discussion

The above data indicates that the intrinsic strength of pure HAP crystal is quite limited in comparison with other ceramics such as silicon nitride [54]. This is, of course, consistent with the fact the HAP crystal is brittle with an inferior performance to fatigue resistance, and this is the main obstacle to its effective direct use in biomedical applications. These results are pertinent only at the atomic scale, but they constitute the first step towards a full understanding of calcified tissue mechanical behavior through multiscale modeling, since these tissues exhibit scale-dependent organization and properties. Indeed, there has been a flurry of composition-based models for elastic behavior of mineralized collagen fibrils [55–57]. Such models are important since they seek to relate the experimentally determined tissue properties to their component properties. Unfortunately, neither reliable nor complete measurements are available for anisotropic stress–strain–strength properties of biologically derived apatitic mineralite or collagen. The current models invariably utilize elastic moduli measured for apatitic polycrystallites [47], which are not appropriate since the apatitic mineralite in calcified tissue is, typically, a nanocrystal. It also widely accepted that most of the nanocrystalline apatitic mineralites are deposited within the collagen fibril and occupy the axial gaps between the aligned collagen molecules, which are bundled in a staggered fashion [58,59]. The c-axis of the HAP crystals is believed to be parallel to the axial direction of the collagen bundles. The interaction at the collagen/mineral interface must have a significant role in the overall behavior. The nature of the cross-link between collagen and the apatite surface has not been investigated. Plausible atomic models of this interface will contribute to far-reaching understanding of these biocomposites.

One of the main goals of the present paper is to develop methods and strategies for realistic modeling of bone and dentin materials since these materials have structures and properties far more complicated than pure bioceramic crystals. For example, solid-state NMR data shows that the OH^- content of human cortical bone is only 20% of that in HAP which will lead to very different mechanical properties and defect behaviors [60]. Si-substituted HAP shows

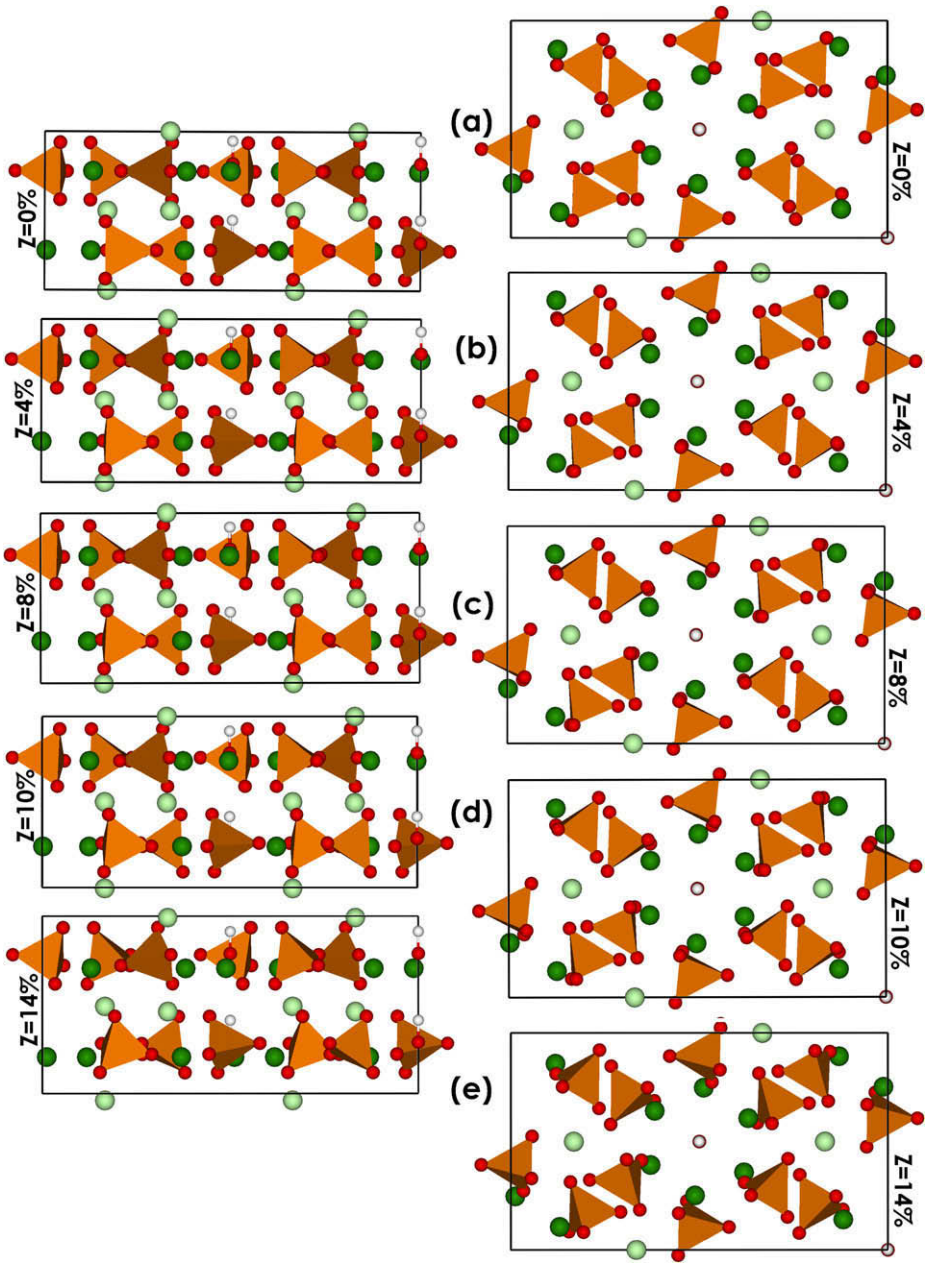

Fig. 5. Evolution of structure as a function of z-axis tensile strain ε_{zz} in the y–z plane of the orthorhombic cell. Left panel: viewed in the y–z plane. Right panel: viewed in the x–z plane. (a) 0%, (b) 4%, (c) 8%, (d) 10% and (d) 14%.

a significant increase in the rate of bone apposition [61] and an increase in vivo bioactivity. Koester et al. [62] showed that the true toughness of human cortical bone is very different from that reported in the literature because of the past failure to account for the orientation-dependent mechanical response.

It is known that there are two types of carbonated HAP. In A(B) type, the carbonate substitution occurs at the hydroxyl (phosphate) site. The B-type carbonated HAP is more relevant to mineralites in bone and dental enamel [15]. The carboxyl groups are the most common functional groups in bio-organic polymers that can react with HAP. They modify the underlying crystal structure and symmetry and obviously affect the mechanical properties. Composite materials of HAP and tetra-calcium phosphates can improve the mechanical properties of HAP [63]. Using the computational approach demonstrated in this paper for pure stoichiometric HAP, a more realistic modeling and investigation of the mechanical properties of composite bioceramics can be envisaged.

5. Conclusions

In conclusion, we have performed calculations of the mechanical properties and carried out a theoretical tensile experiment on perfect HAP crystal using an ab initio tech-

nique. Quantitative parameters for elastic constants and bulk structural parameters are obtained. These values are compared with a variety of measured data and can serve as the upper limit for the mechanical properties of bio-apatites. Theoretical tensile tests show that there exists considerable anisotropy in the stress–strain behavior under both uniaxial and biaxial loads. It is also shown that the deformation behavior is manifest in the rotation of PO_4 tetrahedra with concomitant movements of both the columnar and axial Ca ions under strain. These structural changes during loading result in a vastly different anisotropy of the failure behavior, which is in contrast to the anisotropy of the elastic behavior. These findings are discussed in the context of using this approach to model bioceramic composites related to mineralized tissues in dentin and bones.

The mechanical properties derived from ab initio studies will also have a direct impact on developing larger-scale models of mineralized tissues that can be used to investigate a host of biomedical issues related to load transfer in the muscoloskeletal system. For example, our current knowledge of how damage develops at the building-block levels of dentin and calcified tissue under combined biochemomechanical loading is limited. Similarly, we have incomplete knowledge of the guiding characteristics of tissue-engineered constructs that will replace/restore damaged/diseased hard tissues such as dentin and calcified cartilage that do not regenerate. Computational modeling based on accurate ab initio studies can provide the information on fundamental properties and help in developing a keen understanding of many urgent biomedical problems that affect the aging population.

Acknowledgments

This work is supported by the US Department of Energy under the Grant No. DE-FG02-84DR45170. This research used the resources of NERSC supported by the Office of Science of DOE under the Contract No. DE-AC03-76SF00098. A.M. is partially supported by NSF grant CMS-0506297.

References

[1] Elliott J. Biological apatites. In: Elliott JC, editor. Structure and chemistry of the apatites and other calcium phosphates. Amsterdam: Elsevier; 1994.
[2] Hench LL, Wilson J. Bioceramics. MRS Bull 1991;16(9):62–74.
[3] Currey JD. Three analogies to explain the mechanical properties of bone. Biorheology 1964;2:1–10.
[4] Katz JL. Hard tissue as a composite material. 1. Bounds on elastic behavior. J Biomech 1971;4(5):455.
[5] Wainwright SA. Mechanical design in organisms. Princeton, NJ: Princeton University Press; 1982.
[6] Currey J. Bones, structures and mechanics. Princeton, NJ: Princeton University Press; 2002.
[7] Cowin SC. Bone mechanics. 2nd ed. Boca Raton, FL: CRC Press; 2001.
[8] Collins M, Hunt D, Atherton MAE. Optimisation mechanics in nature. Southampton: WIT Press; 2004.
[9] Ottani V, Martini D, Franchi M, Ruggeri A, Raspanti M. Hierarchical structures in fibrillar collagens. Micron 2002;33(7–8):587–96.
[10] Rho JY, Kuhn-Spearing L, Zioupos P. Mechanical properties and the hierarchical structure of bone. Med Eng Phys 1998;20(2):92–102.
[11] Gruner JW, McConnell D, Armstrong WD. The relationship between crystal structure and chemical composition of enamel and dentin. J Biol Chem 1937;121(2):771–81.
[12] LeGeros RZ. Calcium phosphates in oral biology and medicine. Basel: Karger; 1991.
[13] Mann S. Biomineral types and functions. In: Mann S, editor. Biomineralization, principles and concepts in bioinorganic materials chemistry. Oxford: Oxford University Press; 2001.
[14] Al-Jawad M, Steuwer A, Kilcoyne SH, Shore RC, Cywinski R, Wood DJ. 2D mapping of texture and lattice parameters of dental enamel. Biomaterials 2007;28(18):2908–14.
[15] Sakae T. Variations in dental enamel crystallites and micro-structure. Oral Biosci 2006;48(2):85–93.
[16] Boskey A. Variations in bone mineral properties with age and disease. Musculoskelet Neuronal Interact 2002;2:532–4.
[17] Akkus O, Adar F, Schaffler MB. Age-related changes in physicochemical properties of mineral crystals are related to impaired mechanical function of cortical bone. Bone 2004;34(3):443–53.
[18] Zahn D, Hochrein O, Kawska A, Brickmann J, Kniep R. Towards an atomistic understanding of apatite-collagen biomaterials: linking molecular simulation studies of complex-, crystal- and composite-formation to experimental findings. J Mater Sci 2007;42(21):8966–73.
[19] Marangos O, Misra A, Spencer P, Bohaty B, Katz JL. Physicomechanical properties determination using microscale homotopic measurement: application to sound and caries-affected primary tooth dentin. Acta Biomater 2008;10:023.
[20] Oyen ML, Ferguson VL, Bembey AK, Bushby AJ, Boyde A. Composite bounds on the elastic modulus of bone. J Biomech 2008;41(11):2585–8.
[21] Gupta HS, Schratter S, Tesch W, Roschger P, Berzlanovich A, Schoeberl T, et al. Two different correlations between nanoindentation modulus and mineral content in the bone–cartilage interface. J Struct Biol 2005;149(2):138–48.
[22] Chen J, Ouyang L, Rulis P, Misra A, Ching WY. Complex nonlinear deformation of nanometer intergranular glassy films in β-Si3N4. Phys Rev Lett 2005;95:256103.
[23] Ching WY, Chen J, Rulis P, Ouyang L, Misra A. Ab initio modeling of clean and Y-doped grain boundaries in alumina and intergranular glassy films (IGF) in β-Si3N4. J Mater Sci 2006;41:5061–7.
[24] Ching W, Rulis P, Ouyang L, Misra A. Ab initio tensile experiment on a model of intergranular glassy film in β-Si3N4 with prismatic surfaces. Appl Phys Lett 2009;94(6), 051907-051901-051903.
[25] Misra A, Ouyang L, Chen J, Ching WY. Ab initio calculations of strain fields and failure patterns in silicon nitride intergranular glassy films. Philos Mag 2007;87(25):3839–52.
[26] Kim JY, Fenton RR, Hunter BA, Kennedy BJ. Powder diffraction studies of synthetic calcium and lead apatites. Austr J Chem 2000;53(8):679–86.
[27] Raynaud S, Champion E, Bernache-Assollant D, Laval JP. Determination of calcium/phosphorus atomic ratio of calcium phosphate apatites using X-ray diffractometry. J Am Ceram Soc 2001;84(2):359–66.
[28] Calderin L, Stott MJ, Rubio A. Electronic and crystallographic structure of apatites. Phys Rev B 2003;67(13).
[29] Rulis P, Ouyang L, Ching WY. Electronic structure and bonding in calcium apatite crystals: hydroxyapatite, fluorapatite, chlorapatite, and bromapatite. Phys Rev B 2004;70(15).
[30] Rulis P, Yao HZ, Ouyang LZ, Ching WY. Electronic structure, bonding, charge distribution, and X-ray absorption spectra of the (0 0 1) surfaces of fluorapatite and hydroxyapatite from first principles. Phys Rev B 2007;76(24).
[31] Terra J, Jiang M, Ellis DE. Characterization of electronic structure and bonding in hydroxyapatite: Zn substitution for Ca. Philos Mag A 2002;82(11):2357–77.

[32] Astala R, Stott M. First-principles study of hydroxyapatite surfaces and water absorption. Phys Rev B 2008;78, 075427-075421-075411.
[33] Corno M, Busco C, Bolis V, Tosoni S, Ugliengo P. Water absorption on stoichiometric (0 0 1) and (0 1 0) surfaces of hydroxyapatite: a periodic B3LYP study. Langmuir 2009;25(4):2188–98.
[34] Ma XY, Ellis DE. Initial stages of hydration and Zn substitution/occupation on hydroxyapatite (0 0 0 1) surfaces. Biomaterials 2008;29(3):257–65.
[35] Kresse G, Hafner J. Ab-initio molecular-dynamics for open-shell transition-metals. Phys Rev B 1993;48(17):13115–8.
[36] Kresse G, Furthmuller J. Efficiency of ab initio total energy calculation for metals and semiconductors using plane wave basis set. Comput Mat Sci 1996;6:15–50.
[37] Perdew J, Burke K, Eerzerhof M. Generalized gradient approximation made easy. Phys Rev Lett 1995;77:3865–9.
[38] Yao HZ, Ouyang LZ, Ching WY. Ab initio calculation of elastic constants of ceramic crystals. J Am Ceram Soc 2007;90(10):3194–204.
[39] Voigt W. Lehrbuch der Kristallpysik. Leipzig: Taubner; 1928.
[40] Reuss A, Angnew Z. A calculation of the bulk modulus of polycrystalline materials. Math Meth 1929;9:55.
[41] Hill R. The elastic behavior of a crystalline aggregate. In: Proceedings of the physical society; 1952.
[42] Ogata S, Umeno Y, Kohyama M. First-principles approach to intrinsic strength and deformation of materials: perfect crystals, nano-structures, surfaces and interfaces. Modell Simul Mater Sci Eng 2009;17, 013001-013001-013033.
[43] Chen J, Xu YN, Rulis P, Ouyang LZ, Ching WY. Ab initio theoretical tensile test on Y-doped Sigma-3 grain boundary in alpha-Al2O3. Acta Mater 2005;53(2):403–10.
[44] Snyders R, Music D, Sigumonrong D, Schelnberger B, Jensen J, Schneider JM. Experimental and ab initio study of the mechanical properties of hydroxyapatite. Appl Phys Lett 2007;90(19).
[45] Hearmon RFS. An introduction to applied anisotropic elasticity. London: Oxford University Press; 1961.
[46] Lees SRF. Anisotropy in hard dental tissues. J Biomech 1972;5:557–66.
[47] Gilmore RS, Katz JL. Elastic properties of apatites. J Mater Sci 1982;17(4):1131–41.
[48] Katz JL, Ukrainck K. Anisotropic elastic properties of hydroxyapatite. J Biomech 1971;4(3):221–7.
[49] Nieh TG, Jankowsk AF, Koike J. Processing and characterization of hydroxyapatite coating on titanium produced by magnetron sputting. Mater Res 2001;16:3238–45.
[50] Nelea V, Pelletie H, IIiescu M, Werckmann J, Cracium V, Mihailescu I, et al. Calcium phosphate thin film processing by paulsed laser deposition. Mater Sci Mater Med 2002;13:1167–73.
[51] Guy JL, Mann AB, Kivi KJ, Teaford MF, Weihs TP. Nanoindentation mapping of the mechanical properties of human molar tooth enamel. Arch Oral Biol 2002;47(4):281–91.
[52] Lopes MA, Silva RF, Monteiro FJ, Santos JD. Microstructural dependence of Young's and shear moduli of P2O5 glass reinforced hydroxyapatite for biomedical applications. Biomaterials 2000;21(7):749–54.
[53] Bumrerraj S, Katz JL. Scanning acoustic microscopy study of human cortical and trabecular bone. Ann Biomed Eng 2001;29(12):1034–42.
[54] Ogata S, Hirosaki N, Kocer C, Kitagawa H. An ab initio calculation of the ideal tensile strength of beta-silicon nitride. Phys Rev B 2001;6417(17).
[55] Jager I, Fratzl P. Mineralized collagen fibrils: a mechanical model with a staggered arrangement of mineral particles. Biophys J 2000;79(4):1737–46.
[56] Fritsch A, Hellmich C. 'Universal' microstructural patterns in cortical and trabecular, extracellular and extravascular bone materials: micromechanics-based prediction of anisotropic elasticity. J Theor Biol 2007;244(4):597–620.
[57] Nikolov S, Raabe D. Hierarchical modeling of the elastic properties of bone at submicron scales: the role of extrafibrillar mineralization. Biophys J 2008;94(11):4220–32.
[58] Fratzl P, Gupta HS, Paschalis EP, Roschger P. Structure and mechanical quality of the collagen-mineral nano-composite in bone. J Mater Chem 2004;14(14):2115–23.
[59] Tong W, Glimcher MJ, Katz JL, Kuhn L, Eppell SJ. Size and shape of mineralites in young bovine bone measured by atomic force microscopy. Calcif Tissue Int 2003;72(5):592–8.
[60] Cho GY, Wu YT, Ackerman JL. Detection of hydroxyl ions in bone mineral by solid-state NMR spectroscopy. Science 2003;300(5622):1123–7.
[61] Porter AE, Patel N, Skepper JN, Best SM, Bonfield W. Comparison of in vivo dissolution processes in hydroxyapatite and silicon-substituted hydroxyapatite bioceramics. Biomaterials 2003;24(25):4609–20.
[62] Koester KJ, Ager JW, Ritchie RO. The true toughness of human cortical bone measured with realistically short cracks. Nat Mater 2008;7(8):672–7.
[63] Greish YE, Brown PW. Formation and properties of hydroxyapatite-calcium poly(vinyl phosphonate) composites. J Am Ceram Soc 2002;85(7):1738–44.